AN EXPERIMENTAL STUDY ON THE BASE FLOW PLUME INTERACTION OF BOOSTER CONFIGURATIONS

A. Henckels, A. Gülhan and D. Neeb
German Aerospace Center (DLR)
Windtunnel Department
Institute of Aerodynamics and Flow Technology
Linder Höhe, 51147 Cologne
Germany

OVERVIEW

The integration of the propulsion component plays a key role in the design process of future launchers. At high altitude, conventional rocket nozzles of fixed geometry operate at a non-adapted state. A substantial aerodynamic problem is the interaction between the highly underexpanded plume and the ambient flow field. This interaction may induce boundary layer separation at vehicle base components going along with a significant rise of boat tail drag and may influence the stability and control effectiveness. In the base region "reverse jets" of the hot gas could cause overheating of external nozzle surfaces. To the same extend as the base flow and the shock structures are unstable, oscillations may stimulate "buffeting".

In order to improve the understanding of the interaction of the nozzle flow with the ambient flow, an experimental study on a scaled model representing the base region of a booster configuration has been carried out at the hypersonic wind tunnel H2K. To distinguish between different physical effects, the geometry of the model was kept as simple as possible, i.e. as a single nozzle configuration. At Mach 5.3 and realistic external flow conditions wall pressure measurements and high speed Schlieren visualizations were performed to study the flow topology of cold and warm nozzle flow at several pressure ratios. Tests with different exhaust gases as Helium and Argon provide information on the influence on the specific heat coefficient.

Among others, the study focuses on the identification of shock oscillations as evaluated from Schlieren images. Recorded spectra provide the dominating oscillation frequencies of the external shock as well as the internal shock, linked to the flow condition of nozzle gas. To support the physical interpretation of flow interactions downstream real nozzles and its potential on buffeting effects the measured frequencies are converted into reduced frequencies.

1. INTRODUCTION

The issue of plume interactions in the base region of space vehicles was brought up after 1950 by NASA. Since that time, this topic was investigated theoretically and experimentally by several authors. Early activities by Love et al. [9] provided comprehensive wind tunnel data of jet boundaries of expanding free jets. At the end of the 60's, Brewer and Carven [1] performed experiments inside a test cell pointing out a reverse jet forming in the base region of a four-engine clustered nozzle configuration. Experimental studies of the rear flow field of ARIANE 5 were performed in France by Reijasse and Délery [11] in 1994.

ESA concentrated activities on this subject in the frame of the FESTIP program by initiating investigations on an axisymetric model configuration with an exhaust nozzle. Associated to this effort, Rubio, Matesanz et al. [12] emphasized the importance of quasi-analytical and engineering methodologies for the prediction of base flow/plume interactions and compared their results with CFD calculations and experimental data from ONERA. At the University of Delft, Scarano et al. [13] carried out detailed wind tunnel measurements on the FESTIP model by means of Particle Image Velocimetry at a free stream Mach number of two and a nozzle exit Mach number of four.

Parallel to the advances in CFD, a growing number of numerical and combined analytical/numerical approaches to that subject can be noted [e.g. 6,8,10]. Nevertheless, the complex 3D base/nozzle flow field with its separated flow regions and its several viscous interactions remains a challenging task for CFD simulation. In particular, experiments remain essential to understand physical effects and their impact on the overall design of future launchers. Therefore, the H2K facility of DLR's Windtunnel Department Cologne has been upgraded in order to carry out complex base flow simulations. The specific test facility capabilities and a long term experience in technology orientated hypersonic research on aerodynamic propulsion components, like inlets and SERN nozzles [e.g. 2,3] are the basis of DLR contribution in that field.

In the frame of this study an experimental study on a generic model has been carried out at hypersonic wind tunnel H2K, in order to improve the understanding of the interaction of the nozzle flow with the base flow. For the experiments a scaled model representing the base region of the Liquid Fly-Back Boosters (LFBB, figure 1) configuration [15,16,17], which is one of the possible future booster options for Ariane, has been designed. To distinguish between different physical effects, the geometry of the model was kept as simple as possible, i.e. as a single nozzle configuration.

During this study after a preliminary test campaign [4], runs with a cold and warm nozzle flow were performed at several pressure ratios and at realistic external flow conditions. Wall pressure measurements and Schlieren visualizations were combined to study the flow topology. Among others, this study focuses on identification of pressure oscillations as evaluated from high speed Schlieren visalisations. Further tests with different exhaust gases as Helium and Argon provide information on the influence of the specific heat coefficient and the temperature itself.

This paper describes first the experimental set-up including the complex internal model design. The main part of the paper is devoted to the experiments and discussion of the results. Finally some concluding remarks and outlook are given.

FIG 1. Liquid Fly-Back Boosters shortly after stage separation at about 50 km altitude [17].

2. EXPERIMENTAL TECHNIQUES

2.1. Experimental set-up and test parameters

The flow field around a scaled afterbody/nozzle model is simulated by the conventional hypersonic blow down wind tunnel H2K at DLR Cologne. This facility features a free stream test section and an arrangement of eight electrical heaters of 5 MW total power in order to study high temperature effects and to avoid condensation of the test gas around the model. The complete heating system has its own control unit, linked to the main control system of H2K.

The test flow is generated by contoured Laval nozzles for Mach numbers of 4.8, 5.3, 6.0, 7.0, 8.7 and 11.2. Different Reynolds numbers can be adjusted by the variation of the stagnation conditions. In order to generate an established flow field, the pressure in the test chamber is decreased by a vacuum sphere. During the test the pressure inside this sphere rises and limits the test duration up to 30 seconds.

To heat the secondary flow, i.e. base model nozzle flow, the H2K was upgraded by an auxiliary electrical resistance heater, installed on the floor parallel to the diffuser of the facility (figure 2). The electrical power of 260 kW is sufficient to heat air at mass flow rates of 0.5 $kg\cdot s^{-1}$ up to 800 K at pressures of about 20 bars. To guarantee a reliable operation and to control the performance of the heater, sensors are integrated to measure internal temperatures at sensitive locations. Air mass flow, static pressure and static temperature at the heater exit are measured and transmitted to the main operation desk (figure 3). Finally, the heated air is injected directly into the wind tunnel model. The whole piping from the heater through the test chamber wall is insulated to reduce heat losses.

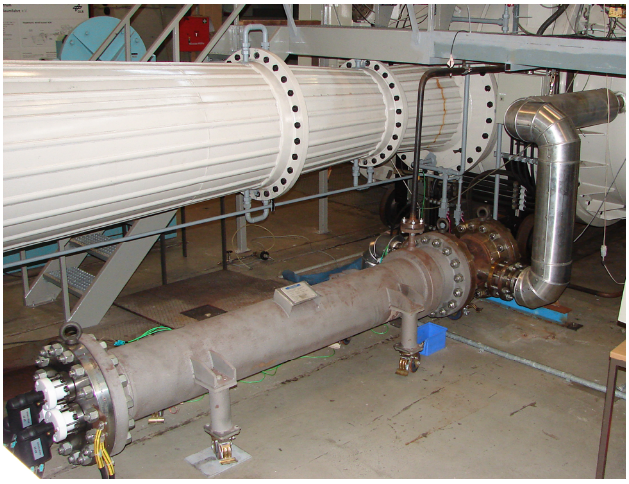

FIG 2. Heater for the nozzle air flow and isolated pipe connected to the H2K test section.

FIG 3. Control panel of the nozzle flow heater integrated into the H2K main operation desk.

In order to simulate the underexpanded operation of a VULCAIN 3 nozzle, the test condition should match the high altitude condition at a typical point of the ascent trajectory of the LFBB reference concept as close as possible. As reference, the condition 138 s after lift off and shortly before booster separation was chosen. The characteristic parameters of that condition, i.e. at a flight altitude of 50 km and a flight Mach number of about 5.3, are given in table 1.

TAB 1. LFBB reference flow condition.

Altitude [km]	50	
Mach number	5.3	
Flight velocity	1750	$m\cdot s^{-1}$
Static pressure	$0.76\cdot 10^{-3}$	bar
Static temperature	271	K
Reynolds number	$1\cdot 10^{5}$	m^{-1}

From an aerodynamic point of view, a precise experimental simulation with scaled models requires to duplicate the most relevant similarity parameters. For instance, Mach and Reynolds number govern the viscous flow effects like boundary layer transition or shear layer establishment. The flight Mach number can simply be reproduced by use of the adequate wind tunnel Laval nozzle. Other important similarity parameters determining the downstream expansion of the plume are the ratio of the nozzle exit pressure to the ambient static pressure as well as the angle of contour divergence at the nozzle exit. Also the momentum ratio between the ambient flow and the gas flow at the nozzle exit should be identical, as this ratio affects the momentum exchange between both sides of the plume shear layer.

Obviously, it is not possible to simulate all these parameters in ground testing, unless identical free stream and exhaust gas temperature and pressure can be realized. In this case the stagnation temperature of more than 3000 K inside the combustion chamber of VULCAIN 3 has to be maintained for several seconds inside the test section of the hypersonic blow down tunnel. This would require major modifications to the facility and its operating procedures. Therefore, this work concentrated on only reproducing the most relevant simulation parameters. For the present simulation, the exit Mach number of the nozzle as well as the ratio of the static pressure at the nozzle exit and the ambient static pressure were identified. Both parameters implied the design of two different nozzle contours [5] providing the test parameters according to table 2.

TAB 2. Reference condition of the nozzle flow.

Nozzle exit:	VULCAIN 3	Nozzle 1	Nozzle 2
Mach number	3.9	3.13	3.88
Expansion ratio ε	35	5	10
Diameter [mm]	1619.8	33.5	47.3
Angle of flow divergence [°]	10.1	10.2	10.0
Total pressure [bar]	139	max. 20	max. 20
Pressure ratio p_{nozzle}/p_∞	401	101	43

It has to be noted, that even with the nozzle designed to reproduce the pressure ratio between nozzle exit and the ambient static pressure, the pressure ratio of the VULCAIN 3 nozzle can not be reached. This is due to the fact that a minimum total pressure of 3 bar is necessary to establish the ambient flow field inside the H2K test section, and that the maximum total pressure of the nozzle of the wind tunnel model is limited to about 20 bar. Thus, the largest achievable pressure ratio p_{nozzle}/p_∞ of about 100 by nozzle 1 is lower than that of VULCAIN 3 nozzle. Nevertheless it is expected, that significant flow features of the underexpanded nozzle flow field are already evident at this lower pressure ratio.

In addition to Mach number and pressure ratio, the total temperature of the nozzle flow is another important simulation parameter. This temperature affects the density of the nozzle jet as well as the viscosity at the shear layers. To understand this influence on the base flow field, the test matrix covers runs with heated exhaust gas. Further runs also cover the use of different exhaust gases as Argon and Helium in order to distinguish between the influence of the specific heat coefficient and the temperature, i.e. viscosity itself.

2.2. Model and measurement technique

The model design in CATIA [7] was based on two guide lines: On one hand, the external model geometry should resemble typical launcher geometries like the LFFB configuration. On the other hand, the external geometry should be as simple as possible in order to support the CFD mesh generation process and to distinguish between physical effects more easily. In addition, the internal model design should compromise several test requirements, e.g. a modular design and a maximum amount of instrumentation. As these tests aim at a simulation of the flow downstream an underexpanded nozzle at high altitude, one nozzle with an adequate mass flow is sufficient to generate relevant plume phenomena of the nozzle cluster [14]. Figure 4 shows the resulting shape of the model with this single nozzle, which is the basis for all accompanying CFD activities.

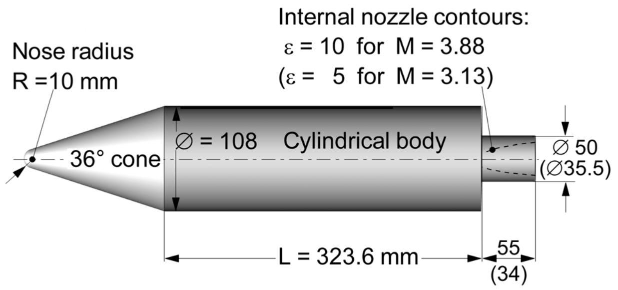

FIG 4. External shape and dimensions of the wind tunnel model (dimensions for nozzle ε = 5 in brackets).

The front section of the model consists of a 36°-cone. In order to demonstrate the influence of the entropy layer development on the establishing boundary layer, tips of different nose radii can be fixed to this cone. A Pitot probe integrated into the nose section allows to measure the free stream condition of the ambient flow. Four circumferential probes at the cones surface support the exact alignment of the model relative to the main flow direction.

The length of the adjacent cylindrical model section is 323 mm, so that the boundary layer develops over a total length of about 0.5 m, before it separates at the base shoulder. For the nominal test flow condition (Mach 5.3, p_0 = 3 bar and T_0 = 600 K) the Reynolds number of about $1 \cdot 10^6$ guarantees laminar separation at that location. This supports the comparison with prospected results from numerical simulations.

The most challenging design element of the model is the air supply, which is needed to feed a sufficient mass flow into the model. Inside the test section, the cylindrical part of the model is attached to a profiled sting, which contains two parallel ducts to minimize external flow interferences. Starting from cold test condition, the nozzle flow has to be heated up to the desired temperature level. In order to keep the pressure level in the vacuum sphere, i.e. in the test chamber low enough, which is necessary for a reasonable testing time, the equilibrium nozzle flow conditions have to be established within a short time period. To meet these requirements, the thermal losses as well as the heated structural mass have to be as small as possible. Therefore, the design philosophy was to separate the cold external model structure, containing the pressure instrumentation, from the hot pressurized internal components, like ducts, settling chamber and nozzle. As shown in figure 5, the stilling chamber and the nozzle are supported by ceramic rings inside the cold structure, which are attached to a spring to compensate the thermal extension.

The stilling chamber and an integrated honeycomb insert are used to reduce the turbulence generated by the manifold of the air supply. The maximum pressure inside this chamber is limited to 20 bars. Downstream of the insert, the stagnation condition of the nozzle flow is measured by a thermocouple and a Pitot probe.

Contrary to the bell shaped external contour of real rocket nozzles, the model nozzles are designed with a cylindrical external contour in order to allow the installation of pressure sensors in the nozzle wall. Further pressure sensors are integrated in the model base and in the base shoulder to gather detailed information on the external base flow.

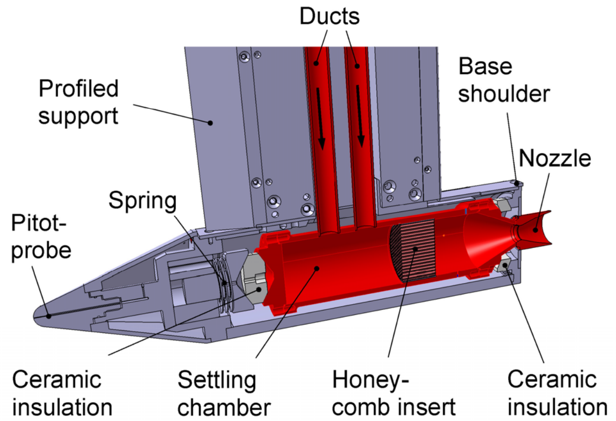

FIG 5. Thermal insulation between the external structure and the hot internal components of the model.

The model installed in the test section of the H2K facility is shown in figure 6. During a run, flow establishment around the model can be monitored by sensitive coincidence Schlieren optics. Parallel, image sections are recorded by a high speed camera (PHOTRON, Ultima APX-RS) at frequencies up to 20 kHz. At selected locations contrast fluctuations taken from these scenes are evaluated by FFT analysis in order to detect flow oscillations.

Information about the entire stationary Pitot pressure distribution downstream the nozzle is gained by a Pitot rake equipped with 14 pipes of 1 mm diameter (figure 7). To support assumptions about the wall temperature condition for numerical simulations, the temperature on the model surface is recorded by an infrared camera system (AGEMA, ThermaCAM SC3000 NTS) at 60 Hz.

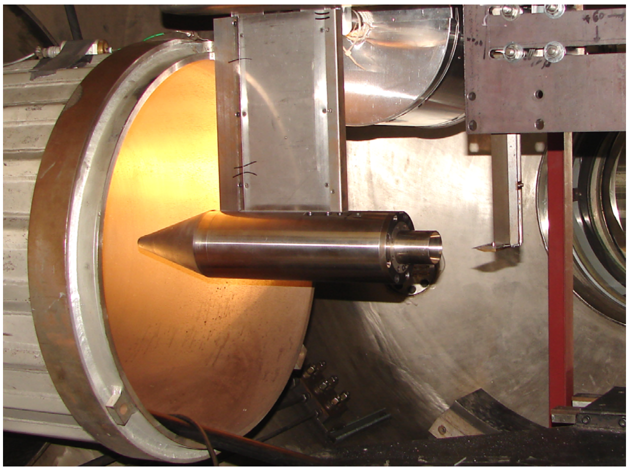

FIG 6. Model installed inside H2K test section.

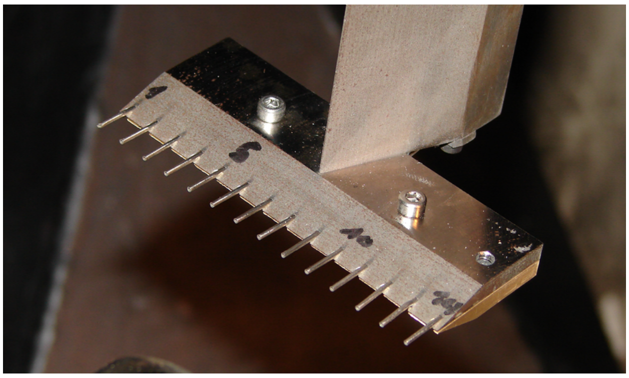

FIG 7. Rake with 14 Pitot probes of 1 mm diameter downstream the nozzle.

3. RESULTS

3.1. Wall pressure and temperature distribution

In order to extract specific flow field features for a physical interpretation, defined test cases with a comprehensive set of flow data are required. For the definition of the boundary conditions of CFD simulations the model wall temperature, the state of the boundary layer flow as well as pressure coefficients at certain model positions (figure 8) are necessary.

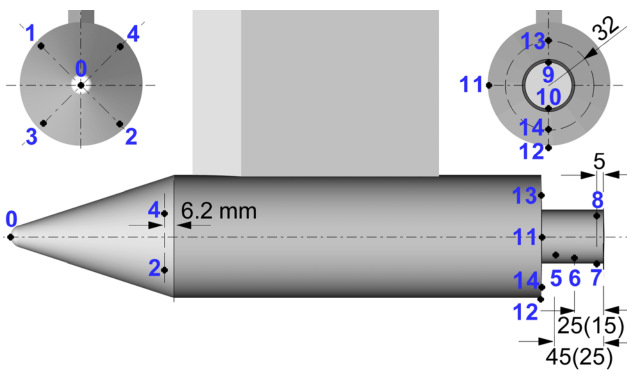

FIG 8. Location of the pressure orifices (blue) for nozzle $\varepsilon = 10$ (nozzle $\varepsilon = 5$ in brackets).

The flow parameters and pressure coefficients for selected test cases are given in tables 3 and 4. The small deviation of about 3 % of the pressure coefficients at positions no. 1 to 4 demonstrates the perfect alignment of the model to the wind tunnel flow. The interpretation of the pressure coefficients no. 5 to 8, measured on the external nozzle contours, naturally suffers from the relatively low pressure levels in this region. At this point the interpretation of the base flow topology will be supported by numerical analysis later.

TAB 3. Flow conditions for selected runs.

Run no.	1	2	3	4
Free stream condition				
M_∞	5.27	5.28	5.28	5.27
Re_∞ [10^6 m^{-1}]	2.82	3.05	3.18	2.86
$T_{0\,\infty}$ [K]	584	578	561	581
$P_{0\,\infty}$ [bar]	3.24	3.44	3.44	3.25
Nozzle flow				
ε	10		5	
Test gas	Air		Air	Argon
M_{exit}	3.88		3.13	3.81
$T_{0\,nozzle}$ [K]	290	710	292	292
$Re_{D\,nozzle}$ [10^6]	4.7	1.3	4.8	6.2
p_{nozzle} / p_∞	34.8	33.4	94.7	30.0
p_{Pitot} / p_0	0.051	0.051	0.051	0.051

TAB 4. Pressures coefficients for selected runs.

Run no.		1	2	3	4
Measured pressure coefficients					
External flow	cp_1	0.214	0.223	0.218	0.216
	cp_2	0.221	0.230	0.213	0.212
	cp_3	0.217	0.225	0.209	0.207
	cp_4	0.214	0.219	0.217	0.214
Nozzle contour	cp_5	-0.009	0.011	-0.006	-0.006
	cp_6	-0.008	0.008	-0.007	-0.008
	cp_7	-0.010	0.003	-0.004	-0.007
	cp_8	-0.008	0.016	-0.010	-0.010
Internal flow	cp_9	3.162	2.968	7.650	3.182
	cp_{10}	2.885	2.746	7.544	3.163
Base	cp_{11}	0.005	0.023	0.000	-0.003
	cp_{12}	-0.001	0.010	-0.006	-0.006
	cp_{13}	-0.004	0.018	-0.010	-0.008
	cp_{14}	-0.005	0.016	-0.008	-0.005

Evaluating the differences between pressure coefficients no. 7 and no. 8 measured at opposite positions, an influence of the sting might be concluded. This sting influence is also confirmed by pressure coefficient no. 14, which is lower in comparison to pressure coefficient no. 13. Note that the measured pressure levels are relatively low and thus are subject to a high sensitivity to the model geometry. For a final judgment of the sting influence, Pitot pressure surveys of the flow field downstream of the model will be shown later. Nevertheless, it is expected that the measured pressure coefficients at the lower model side are not affected by the sting influence.

The flow inside the stilling chamber of the model is reduced to relative low flow velocity (Mach 0.03). Therefore, and because of the installed honeycomb insert, a rather homogenous flow field entering the nozzle is expected. In contrast with this, a remarkable difference in the pressure coefficients no. 9 and no. 10, measured at opposite sides inside the nozzle near its exit plane, became obvious. These differences correspond to Mach number deviation in the order of about ±1%, which is still acceptable. A detailed check of the internal nozzle contour by precise measurement instrumentation showed, that the nozzle geometries were nearly axis symmetric. Additionally, enlarged Schlieren images proved a nearly perfect symmetrical nozzle flow pattern.

CFD simulations require assumptions about the temperature condition at the model surfaces, i.e. an adiabatic or isothermal wall at a certain temperature level. The wind tunnel model is machined from steel, having a significant high thermal conductivity. During the entire test run, a nearly homogenous surface temperature on particular model parts is found from infrared images. The wall temperature of the cylindrical model is mainly influenced by the stagnation temperature of the ambient flow. The wall temperature of the nozzle results mainly from internal heat conduction, and therefore is controlled by the stagnation temperature of the nozzle flow.

An evaluation of exact temperatures requires knowledge about the surface emissivity, which for the oxidized steel surface is specified near to 0.65. In table 5 measured temperatures are referred to relevant stagnation temperatures. These data support clearly the isothermal wall assumption.

TAB 5. Measured model wall temperatures for run no. 2 of table 3 (emissivity 0.65).

Model component	Test duration [sec]	T_{wall} [K]	$T_{0\,ref.}$ [K]	$T_{wall}/T_{0\,ref}$
Cylindrical body	1	318	$T_{0\,\infty}$ = 578	0.55
	20	323	$T_{0\,\infty}$ = 578	0.56
Nozzle	1	436	$T_{0\,nozzle}$= 710	0.61
	20	455	$T_{0\,nozzle}$= 710	0.64

3.2. Base flow topology and support arm influence

As the vehicle passes the atmosphere, the ambient pressure decreases to low levels. At static pressures corresponding to 50 km altitude, the model nozzle operates at strongly underexpanded condition, which leads to the flow topology sketched in figure 9: At the rear of the cylindrical model, the boundary layer separates as free slip line, forming a small expansion at the base shoulder. This slip line encloses the low pressure base flow region with embedded subsonic vortices. Further downstream, near to the plane of the nozzle exit, the slip line interacts with the viscous shear layer, which separates the exhaust gas from the ambient flow. Thereby, an external shock is generated, spreading circularly around vehicles rear.

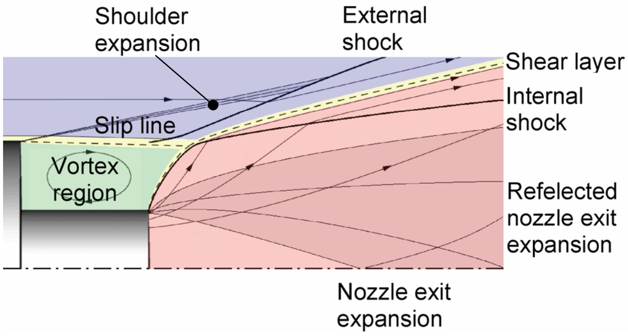

FIG 9. Sketch of the flow structure downstream the model.

At the nozzle exit, the exhausted high pressure gas rapidly expands by generating an expansion fan spreading towards the plume axis. Thereby, particularly at the edge of the nozzle exit, the flow is turned by large angles (see stream lines). In order to adapt the direction of the core flow to the direction of the viscous shear layer, which is positioned by the pressure balance, an "internal shock" still embedded inside the plume gas is generated. As Schlieren images in figure 10 shows, plume features change depending on the sufficient density gradient, which increases by the stagnation pressure of the nozzle flow significantly.

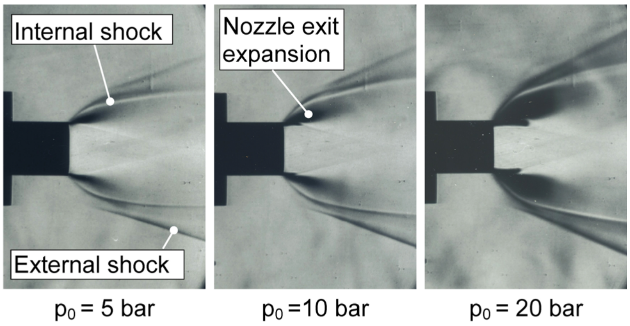

FIG 10. Air plume at different nozzle flow stagnation pressures (Nozzle ε = 10, nominal external flow condition Mach 5.3, p_0 = 3 bar and T_0 = 600 K).

The influence of the ambient flow field on the plume size is stated by runs with the wind tunnel flow turned off and on. Figure 11 shows the corresponding Schlieren images taken at different stagnation pressures of the nozzle (expansion ratio 5), but at constant nominal conditions of the wind tunnel flow. Since only the stagnation pressure of the nozzle flow, and thus the mass flow through the model is increased, the size of the nozzle plume grows.

The model is mounted inside the test section on a profiled support arm, which may disturb the external flow field downstream. The arrangement of the measured Pitot pressure contour and a Schlieren image of the base flow field (figure 12) shows the small influence of the support arm wake on the deformation of the circular external shock, which is visible as the foot print in the pressure contour. Therefore, further relevant flow measurements and high speed flow visualizations focus on the lower model section, where no sting disturbances are detected.

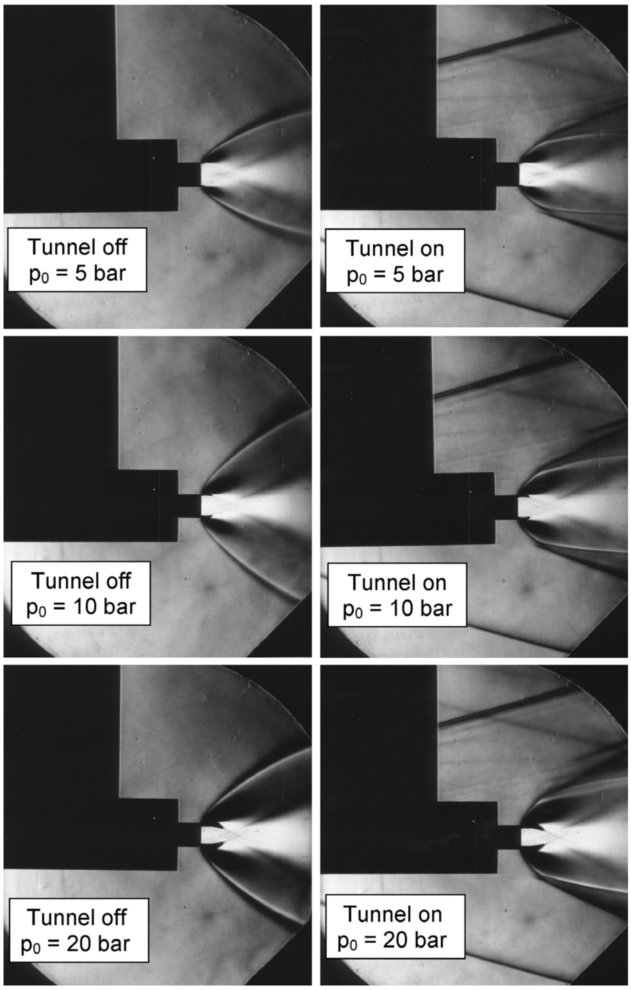

FIG 11. Air plume at different nozzle flow stagnation pressures (Nozzle ε = 5, nominal external flow condition Mach 5.3, p_0 = 3 bar and T_0 = 600 K).

Also, Pitot pressure measurements were performed for different nozzle stagnation temperatures but identical pressure conditions. Gained pressure profiles visualize the nozzle flow core as well as the positions of the internal and external shock (Figure 13). Nevertheless, no significant difference between the profiles of 290 K and 660 K stagnation temperature has been detected.

For the LFBB configuration at 50 km altitude the Reynolds number at the shoulder of the cylindrical base section is about $4 \cdot 10^6$, which leads to a less defined transitional character of the boundary layer. In contrast to this, the nominal free stream test condition of H2K (Mach 5.3, 600 K and 3 bar) guarantees laminar separation at this location.

In order to identify the influence of the boundary layer state, runs at different free stream Reynolds numbers, but at an identical pressure ratio between the static pressure at the nozzle exit and the ambient pressure have been performed. Even at different Reynolds numbers the separating boundary layer leads to an identical after body flow field with the same plume size.

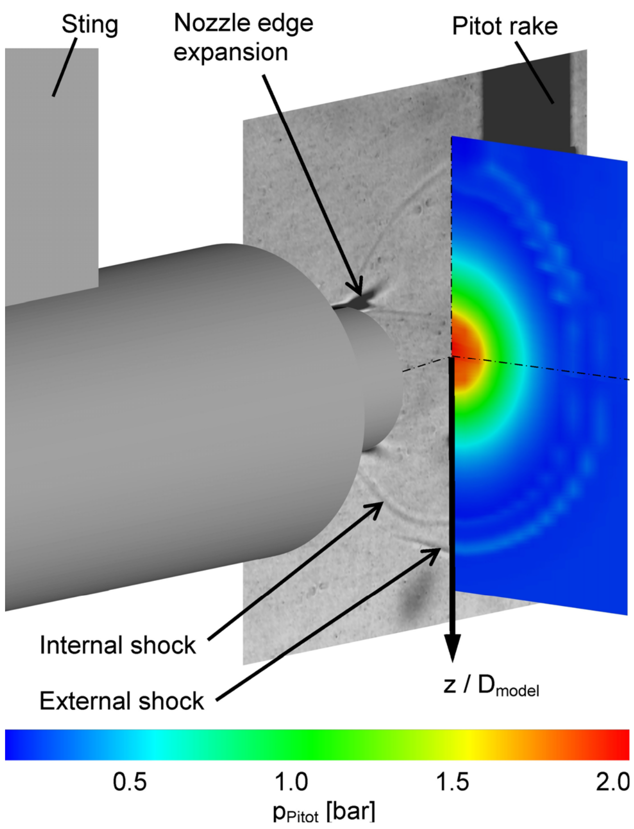

FIG 12. Arrangement of measured Pitot pressure contour and Schlieren image of the base flow field.

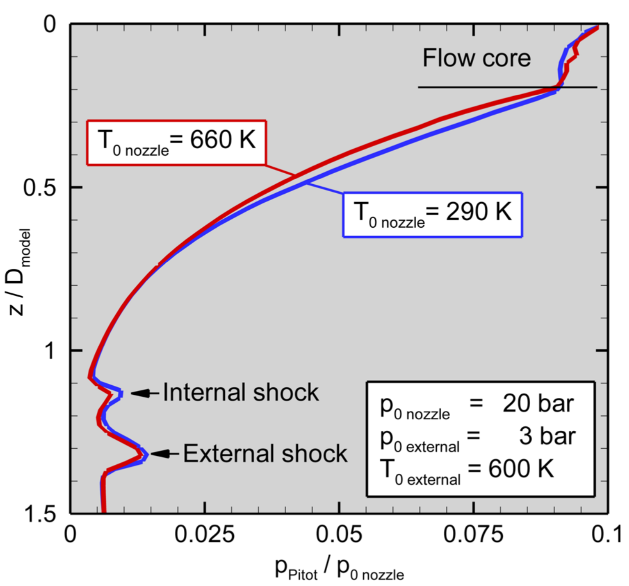

FIG 13. Pitot pressure profile (coordinate see FIG 12) for two nozzle flow stagnation temperatures.

3.3. Effects of different exhaust gases on flow interactions

The propelling gas of real rockets is different than the wind tunnel nozzle of this study, particularly with respect to establishing temperatures and hence the gas property. To gain basic information about the influence of the gas property on the after body flow interactions and to distinguish between the influence of the specific heat coefficient and the temperature itself, runs with different exhaust gases like Argon and Helium are carried out. Expanding these gases through the nozzle, all flow parameters like velocity, temperature and Mach number are affected by the value of the specific heat coefficient. For example, the nominal nozzle exit Mach number increases from about 3.9 for air to about 5.1 for Helium and Argon. Further relevant flow data are indicated by table 6.

TAB 6. Gas properties of Argon, Helium and Air and nominal test flow conditions.

	Ar	He	Air	Air	
Specific heat coefficient	1.67	1.67	1.40	1.40	
Gas constant	208	2077	287	287	
Stagnation temperature	300	300	300	300	K
Stagnation pressure	10	10	10	5	bar
Nozzle exit Mach number	5.1	5.1	3.9	3.9	
Velocity	528	1668	674	674	m/s
Static density	0.55	0.06	0.35	0.17	Kg/m³
Static temperature	32	32	73	73	K
Static pressure	0.036	0.036	0.073	0.037	bar

For these runs, the stagnation pressure of the nozzle flow is adjusted to 10 bar in order to resolve small density gradients by Schlieren optics, particularly of the Helium flow. For comparison to tests with air, two strategies may be followed by adapting the stagnation temperature of the nozzle flow: Either the stagnation pressure of air can be identical to the stagnation pressures of the other gases or an identical ratio of static pressure across the plume shear layer can be adjusted. The latter condition leads to equivalent plume sizes.

The design of the nozzle contour for air encounters the elimination of reflected flow characteristics at the internal wall. Characteristic angles resulting from the specific heat coefficient of Helium and Argon do not match to the geometry, originally designed for air. This leads to internal reflections, which may grow to shock structures, spreading from the nozzle wall forwards the plume axis as visible from Schlieren images.

For an external flow of Mach 5.3, $p_0 = 3$ bar and $T_0 = 330$ K, figure 14 shows plumes formed at identical stagnation pressures (air, 10 bar) or at identical static pressure ratios between internal and external flow (air, 5 bar). For the Argon flow, the static temperature reaches a level well beyond the solidification point. Nevertheless, related flow effects could not be observed from the Schlieren images. It is expected, that the solidification process is time shifted due to the low pressure level and the high flow velocity.

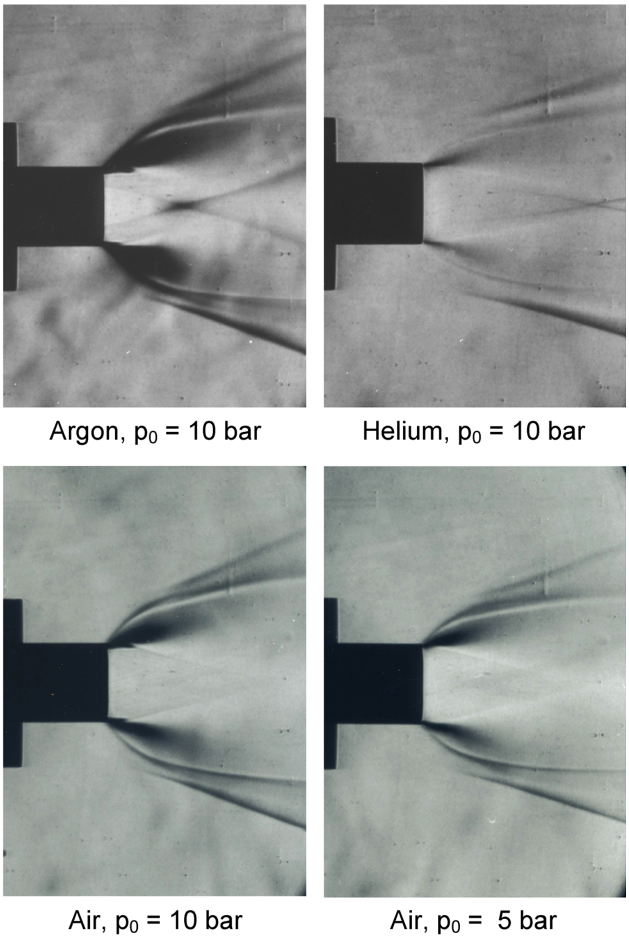

FIG 14 Argon and Helium plumes in comparison with the air plume according to table 6.

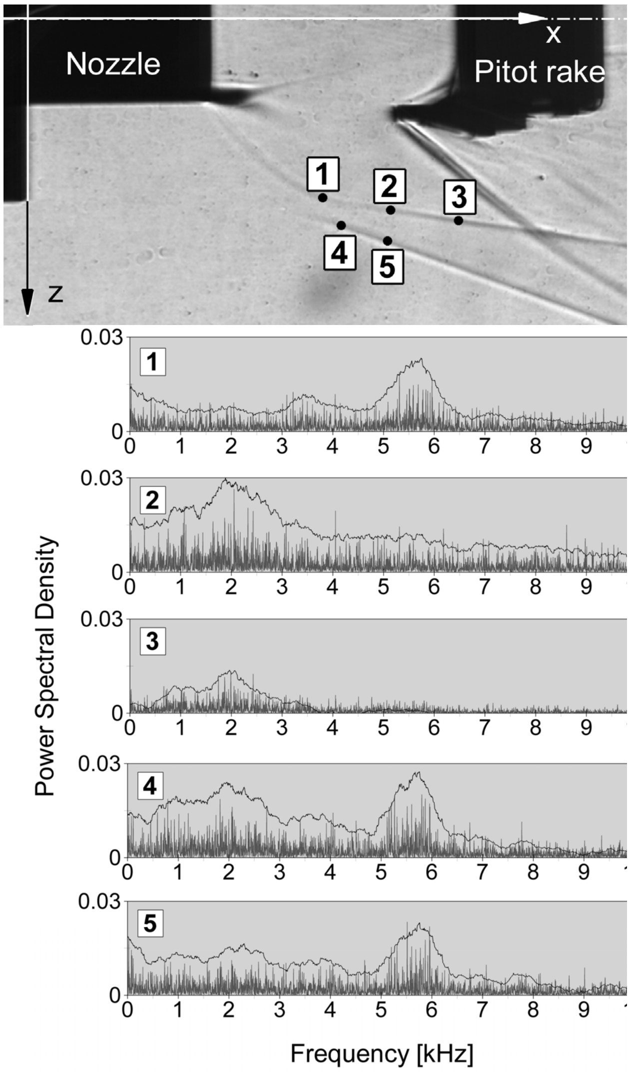

FIG 15. Frequency analyses of the oscillations at selected locations of the internal and external shock.

3.4. Shock oscillations and recorded spectra

The physical interpretation of time-dependent flow phenomena and its potential on buffeting effects ask for an identification of flow oscillations downstream the nozzle. At selected locations, frequency analyses of the internal and external shocks are performed by evaluating oscillations from high speed Schlieren images (figure 15). Thereby, flow conditions of run no. 1, table 5 for a stagnation temperature of the exhausted air of 660 K, are used.

Figure 15 shows measured power spectral densities (peaks) as well as a power spectral density averaged over 500 Hz (line) at different locations. From these data following interpretation seems to be feasible: At position no. 2 and 3 frequencies between around 2 kHz are dominating the oscillation spectrum of the internal shock, which is physically linked to the flow condition of the nozzle gas. The amplitude of this oscillation grows for an increasing distance to the nozzle exit.

Dominating frequencies of the external shock oscillation at position no. 4 and no. 5, which are linked to ambient or base flow field, are found at 5 and 6 kHz. At position no. 1, the influence of the external shock is still weak, so that frequencies between 5 to 6 kHz are weakly pronounced. Further test results with unheated exhaust gas confirmed these interpretations.

In order to transfer the ground testing results to the real flight condition, the reduced frequency $k = 2\,\pi\,f\,D_{ref.}/v_{ref.}$ is computed. A Mach number of 5.3 and a stagnation condition of 3 bars at 600 K leads to a reference velocity, i.e. free stream velocity of $v_{ref.}$ = 1012 m/s. Table 7 shows the results for a model diameter of $D_{ref.}$ = 0.108 m, associated to the coordinates of the evaluated shocks.

TAB 7. Selected locations and results of the frequency analyses.

No.	Location	x [mm]	z [mm]	Frequency f [kHz]	Reduced frequency k
1	Internal shock	88	54	5 - 6	3.4 – 4.0
2	Internal shock	108	57	around 2	around 1.3
3	Internal shock	128	61	around 2	around 1.3
4	External shock	93	62	5 - 6	3.4 – 4.0
5	External shock	107	66	5 - 6	3.4 – 4.0

4. CONCLUSIONS

Successful tests on the interaction between the cold air nozzle flow and hypersonic external flow verify the experimental test concept and the functionality of the instrumentation. Negligible deviations were measured between the pressure coefficients at different positions on the cone of the model and confirmed a perfect model alignment with respect to the free stream direction.

Schlieren images indicated an almost symmetrical nozzle flow. Nevertheless, sting interactions induce fluctuations of the plume shear layer in the upper part of the flow field. Such disturbances are confirmed by Pitot pressure measurements in a plane downstream the model perpendicular to the mean stream direction. Therefore, all further evaluation focus on the lower part of the flow field.

Schlieren images taken with and without wind tunnel flow visualize the plume shear layer as well as established internal and external plume shocks. In order to indicate viscous flow effects, test runs were performed at different free stream Reynolds numbers, i.e. for laminar and transitional separation at the model shoulder. No significant differences in the location of the plume shear layer and the external nozzle shock were identified.

In combination with these Schlieren images, the measured wall pressure distributions at certain locations of the base and nozzle contours can be used as a reference for CFD validation. Surface temperature measurements showed that isothermal wall assumption is relevant for the test condition of this study.

In addition to the Mach number and the nozzle pressure ratio, the total temperature of the nozzle flow is another important simulation parameter. This temperature affects the density of the plume flow as well as the viscosity at the shear layers.

To investigate the influence on the base flow field, tests include runs with heated nozzle flow, i.e. with nozzle flow total temperatures up to 710 K. Further tests with different exhaust gases were carried out to distinguish between the influence of the specific heat coefficient and the temperature itself.

High speed Schlieren imaging combined with adequate evaluation software proved this technique to be an efficient non-intrusive measurement technique for frequency analysis. Disturbances as caused by the design of gauges or by the interaction of the gauges with the flow are completely avoided. From such high speed Schlieren images oscillation frequencies of the internal and external shock were evaluated.

The interpretation of recorded spectra suggests that frequencies around 2 kHz are dominating the internal shock, linked to the flow condition of nozzle gas. Marking oscillations of the external shock, which are linked to ambient or base flow, were found between 5 and 6 kHz. These experimental data will support a physical interpretation of time-dependent flow phenomena downstream rocket nozzles and its potential on buffeting effects.

5. ACKNOWLEDGMENT

The authors gratefully acknowledge the support by the DLR's space program directorate and the Helmholtz Association (HGF) in the frame of a “virtual institute“.

6. REFERENCES

[1] Brewer, E. B., Craven, C. E, Experimental Investigation of Base Flow Field at High Altitude for a Four-Engine Clustered Nozzle Configuration, NASA TN D-5164, Washington, 1969.

[2] Gruhn, P., Henckels, A., Simulation of a SERN/Afterbody Flow Field regarding heated Nozzle Flow in Hypersonic Facility H2K, Contribution to the 13. DGLR-Fach-Symp. published in: Notes on Numerical Fluid Mechanics, Vol. 78, Ch. Breitsamter, B. Laschka et al. (Eds.), pp. 236-243, Springer Verlag 2004.

[3] Henckels, A., Gruhn, P., Experimental Studies of Viscous Interaction Effects in Hypersonic Inlets and Nozzle Flow Fields, in “Basic Research Technologies for Two-Stage-to-Orbit Vehicles”, D. Jacob, G. Sachs, S. Wagner (Eds.), pp. 383-403, Wiley-VCH Verlag, 2005.

[4] Henckels, A.; Gruhn P.; Gülhan A.; First Experimental Results on the Nozzle/Base Flow Interaction for Launcher Configurations, 6th Intern. Symp. on Launcher Technologies, Munich, Nov. 2005.

[5] Herbertz, A., Sippel M., Vorbereitung der Untersuchungen zur Heckströmung und Plume-Entwicklung bei Raumtransportsystemen, DLR-IB 647-2004/04, Köln, 2005.

[6] Houtman, E. M., van der Weide, E., et al., Computational Analysis of Base Flow/Jet Plume Interaction, Proc. of the 3ed European Symposium on Aerothermodynamics for Space Vehicles, Noordwijk, Nov. 1998. ESA SP-426, pp. -605-612, 1998.

[7] Kloft, S., Auslegung eines Windkanalmodells zur Untersuchung der Interaktion zwischen unterexpandierender Düsenströmung und Raketenumströmung, Diplomarbeit, Fachhochschule Koblenz, 2004.

[8] Lüdeke, H., Clavo, J. B., et al., Fluid Structure Interaction at the ARIANE-5 Nozzle Section by Advanced Turbulenc Models, Europ. Conf. on Computational Fluid Dynamics, TU Delft, Netherlands, 2006.

[9] Love, E. S., Grigsby, C. E, et al., Experimental and Theoretical Studies of Axisymmetric Free Jets, NASA-TR-R-6, Washington, 1959.

[10] Reig, J. L., Velázquez, A., et al., Quasi-Analytical Prediction of Base Flow-Plume Interaction, Proc. of the 3ed European Symposium on Aerothermodynamics for Space Vehicles, Noordwijk, Nov. 1998. ESA SP-426, pp. 599-604, 1998.

[11] Reijasse, P., Délery, J., Investigation of the Flow past the ARIANE 5 Launcher Afterbody, Journal of Spacecraft and Rockets, Vol. 31, No. 2, pp. 208-214, 1994.

[12] Rubio, G., Matesanz, A., et al., Prediction of Base Flow/Plume Interaction including 3-D and Real Gas Effects, AIAA Paper 2000-3171, 2000.

[13] Scarano, F., van Oudheusden, B. W., et al., Experimental Investigation of Supersonic Base Plume Interaction by Means of Particle Image Velocimetry, Proc. of the 5th European Symposium on Aerothermodynamics for Space Vehicles, Cologne, 2004. ESA SP-563, pp. 601-607, 2005.

[14] Simmons, F. S., Rocket Exhaust Plume Phenomenology, The Aerospace Press, El Segundo, California, p. 32, 2000.

[15] Sippel, M., Manfletti, C., et al., Technical Development Perspectives of Reusable Booster Stages. AIAA Paper 2003-7057, 2003.

[16] Sippel, M., Klevanski, J., Preliminary Definition of an Aerodynamic Configuration for a Reusable Booster Stage within Tight Geometric Constrains, Proc. of the 5th European Symposium on Aerothermodynamics for Space Vehicles, Cologne, Nov. 2004. ESA SP-563, pp. 21-27, 2005.

[17] Sippel, M.: Concurrent Launcher Engineering at DLR, Concurrent Engineering Workshop, ESTEC, Internet: //www.la.dlr.de/ra/sart/projects/lfbb/lfbb.php.en, 2004.